Supplementary Information

Supplementary Figure Legends

Figure S1. Mitochondrial localization signal (MTS) and recombinant expression of mature human NADK2. A. Prediction of MTS in human NADK2 using MitoFates server (1). **B.** Coomassie staining of recombinant human SeMet-NADK2 (47-442) purified by size-exclusion (Superdex S200) chromatography and used for experimental phasing.

Figure S2. Simulated annealing (SA) omit electron density map for NAD^+ in the active site. SA (2000K to 100K in steps of 100K) was performed in Phenix. Coordinates for NAD^+ were excluded from the SA procedure. F_o-F_c omit maps countered at 4, 5, and 6 sigma are shown.

Figure S3. $2F_o$-F_c electron density map for NADK2. A. Electron density map from SA run (2000K to 100K in steps of 100K) for chain A (left panel). NAD^+ is colored green. **B.** Close-up view of electron density near the active site.

Figure S4. Observation of NADK2 homodimer in the crystal structure. A, Asymmetric unit in NADK2 crystal structure (PDB ID 7N29) depicts four copies of NADK2. Each copy represents a single chain from dimeric NADK2. **B**, Visualization of NADK2 homodimers by adding symmetry mates (PyMOL A→generate→symmetry mates).

Figure S5. Size exclusion chromatography with NAD^+ added. A, Elution trace for NAD^+. A260 and A280 traces show absorbance at 260 nm and 280 nm. **B**, Elution trace for 70 μM NADK2 47-442 WT mixed with 1 mM NAD^+ in reaction buffer with 20 mM HEPES pH 7.4, 300 mM NaCl, 2 mM MgCl2, 10% glycerol and 5 mM DTT. Mixture was pre-incubated on ice for 30 min followed by injection to S200 size-exclusion chromatography column. **C**, Migration of NADK2 in the absence of NAD^+.

Figure S6. Analysis of NAD^+/NADH substrate preference by human NADK and NADK2 observed in direct assay. A. Kinase activity of human NADK and NADK2 (amino acids 47-442) in the presence of NAD^+ or NADH substrates. Assays were performed with 8.75 mM NAD^+ or NADH. Reactions were conducted at 37 ºC and contained either 1 μM NADK or 11.1 μM NADK2, and trace γ-^{32}P-ATP. Substrates (ATP) and Products ($NADP^+$ and NADPH) are marked on the gel. **B.** Quantification of data in panel (A). Error bars show S.E. from the experimental repeats in panel (A).

Figure S7. Measurement of ATP and NAD^+ substrate parameters for NADK2 and NADK. A. ATP titration profile for NADK and NADK2. Assays were performed with 8.75 mM NAD^+, 1 μM NADK or 12.5 μM NADK2, and trace γ-^{32}P-ATP. Reactions were conducted at 37 ºC. Titration was performed using 1:1 ATP-Mg^{2+} complex. **B.** NAD^+ titration profile as in Fig. 5B, but with 2 mM cold ATP background. Reactions were conducted as in panel (A).

Figure S8. Kinase activity analysis of NADK2 mutants. Independent replicates related to Fig. 5C.

Figure S9. Crystal packing dimer observed in a structure of human NADK (PDB ID 3PFN). N-termini of two neighboring copies are swapped in-trans, presumably stabilizing the dimer. Akt kinase phosphorylation sites are located in the N-termini (2).

Materials and Methods

Cloning

The coding region of full-length human NADK2 (residues 1-442) was codon-optimized for expression in *Escherichia coli* and synthesized by Genewiz. The coding region of full-length human NADK (residues 1-447) was amplified by PCR from an in-house cDNA library using A549 human lung epithelial cells. DNAs containing the coding regions were cloned in pGEX-6P bacterial expression vector (GE Healthcare Life Sciences). Deletion and point mutants were generated by site-directed mutagenesis as previously described (3). All constructs used in this study were verified by DNA sequencing.

Protein Purification

Vectors encoding recombinant proteins were transformed to *Escherichia coli* BL21 (DE3)-CodonPlus RIPL (Agilent Technologies). Cells were grown to an OD600 between 0.8 and 1.0 in Luria-Bertani medium at 37 ^{o}C. For selenomethionine-derived NADK2 protein, pGEX-6P vector was transformed into B834 (DE3) competent cells (Novagen) and grown to an OD600 of 1.0 in M9 media supplemented with 18 amino acids, except for Cys and Met. Media contained 0.4% glucose, 1 mM $MgSO_4$, 0.1 mM $CaCl_2$, 0.5 mg/ml Fe-ammonium sulfate, and MEM Vitamin Solution (Gibco). Protein expression was then induced with 0.4 mM isopropyl-β-D-thiogalactopyranoside (IPTG) at 22 ºC overnight. The cells were pelleted at 4,600 × *g* for 25 min, resuspended in lysis buffer (20 mM HEPES pH 7.4, 600 mM NaCl, 2 mM $MgCl_2$, 1 mM EDTA, 10% (vol/vol)

glycerol, 5 mM DTT, 1% TX-100 and Roche cOmplete protease inhibitor), and lysed on EmulsiFlex C3 (Avestin).

Protein purification was performed at 4 ºC. Crude lysates were clarified by centrifugation at 35,000 × *g* for 30 min, followed by ammonium sulfate (1.64 M) precipitation. Clarified lysates were affinity-purified using glutathione Sepharose (GE Healthcare Life Sciences). The GST tag was removed with Prescission protease (A.G. Scientific). In order to remove possible kinase contaminants from *E.coli*, all protein solutions were further purified by MonoS, then by MonoQ ion-exchange chromatography, and lastly, by Superdex 200 Increase 10/300 GL size-exclusion chromatography (GE Healthcare Life Sciences). Size exclusion buffer contained 20 mM HEPES (pH7.4), 300 mM NaCl, 2 mM $MgCl_2$, 10% (vol/vol) glycerol, and 5 mM DTT. All proteins were purified to ≥ 95% purity. Concentrations were measured by UV 280 spectrophotometry, and adjusted to extinction coefficients determined by protein sequence. Four pieces of evidence suggest that purified protein is free of bound ligands. First, electron density for ATP was absent in the crystal structure even though excess of ATP (9 mM) was added to crystallization conditions. The labile ATP binding to the enzyme indicates that ATP is certainly lost from NADK2 during purification. Second, NADK2 did not crystallize until NAD^+ was added indicating that initially bound NAD^+ was absent. Third, the addition of a physiologically relevant concentration of NAD^+ to NADK2 did not change its size exclusion chromatography migration profile (Fig. S5). Fourth, we observed normal hyperbolic dose response of NADK2 activity vs NAD^+ (Fig. 5), which indicates that the enzyme active site is unoccupied. If the active site initially contained bound substrate (NAD^+), NADK2 activity would not show a NAD^+ dose response. If the

active site was initially occupied with bound product (NADP), the only scenario for NADP to survive purification would be for NADP to have a slow rate constant for release (k_{off} << 0.1 s^{-1}), which directly contradicts with fast multiple-turnover rate constant for NADP synthesis reaction that we measured (k_{cat} > 1 s^{-1}, Fig. 5B; we note that k_{off} for product release cannot be smaller than k_{cat}).

Gel filtration migration assay

NADK or NADK2 recombinant protein constructs were injected on a Superdex S200 column (GE Healthcare Life Sciences). Size-exclusion chromatography was run at 4 ºC in buffer containing 20 mM HEPES (pH 7.4), 300 mM NaCl, 2 mM $MgCl_2$, 10% (vol/vol) glycerol, and 5 mM DTT.

Radioisotope Kinetics Assay

Recombinant NADK and NADK2 were mixed with reaction buffer (50 mM Tris pH 8.0, 100 mM NaCl and 10 mM $MgCl_2$) and 8.75 mM NAD^+. Samples were pre-incubated at 37°C for 5 min. One microliter of solution with trace amount of γ-^{32}P-ATP (Perkin Elmer) in 10 mM TRIS-chloride buffer (pH 7.6) was rapidly mixed to start the reaction. Time courses were performed at 37°C, and stopped at indicated times with the addition of quencher solution (90% formamide, 2.5% glycerol, 0.01% SDS, 0.01% bromophenol blue, 0.01% xylene cyanol, 1 mM EDTA). The samples were heated for 3 min at 95 ºC, and analyzed by 20% urea-polyacrylamide gel. Gel images were visualized by

phosphorimaging on a Typhoon FLA 7000 (GE). Product and substrate intensities were quantified using GelQuant.NET (Biochem Lab Solutions).

NADK2•NAD^+ Co-crystallization

Crystallization drops contained 1.78 mg/ml of selenomethionine-derived NADK2 47-442, 9 mM ATP, and 70 mM NAD^+ (Sigma). Co-crystals were grown using the hanging drop vapor diffusion method by mixing the crystallization complex 1:2 with reservoir solution (200 mM $MgCl_2$ and 17% (w/v) PEG 3,350) at 20°C. Larger crystals were obtained by streak-seeding into reservoir solution containing 200 mM $MgCl_2$ and 4% (w/v) PEG 3,350. Crystals were cryoprotected using 15% ethylene glycol, 17% (w/v) PEG 3,350 and 200 mM $MgCl_2$, then frozen in liquid nitrogen.

X-Ray Data Collection and Structure Determination

X-ray data were collected at NSLS-II beamline FMX from crystals containing selenomethionine-substituted protein. Data were collected in a single-wavelength anomalous scattering experiment at a wavelength of 0.9793 Å at the selenium K edge and processed with XDS (4) and AIMLESS (5) (Table S1). The selenium substructure was determined by SHELXD (6) and experimental phases calculated with SHELXE (7). Iterative model building with COOT (8) into experimentally-phased and model-phased maps and refinement with PHENIX (9) incorporated non-crystallographic symmetry restraints for three initial copies of the monomer. Towards the end of refinement it became apparent that a fourth monomer chain was present, at reduced occupancy,

verified by the presence of weak selenium peaks in the model-phased anomalous difference map, and also by the presence of unexplained density in the $2F_o$-F_c map. A fourth monomer was placed in the asymmetric unit with occupancy of 0.44, exhibiting correspondingly weaker density in both experimental and $2F_o$-F_c electron density maps. The final model has good agreement between experimental data and the model, with excellent stereochemistry (Table S1).

X-ray structure visualization and analysis

Structure images were generated using UCSF Chimera (10) and PyMol (DeLano Scientific build). Sequence conservation and 3D conservation mapping was conducted using SEQMOL-Kd (BiochemLabSolutions.com).

Bioinformatics

The α8-α9 insert was identified computationally using conserved flanking regions as sequence anchor points. Insert sequences with the flanking regions were extracted from FASTA-formatted protein sequences obtained from Expasy Blast server (11) using the following regular expression: [TS][G][TS]G[SC][TRSK][AS].{0,10}[WR].{30,100}[VIL][RC][DEN].[IMVLH]. Sequence hits were finalized by trimming the flanking regions.

Error analysis

Unless specified, error bars in solution assays show S.E. from three independent experiments.

Table S1. Data Collection and Refinement Statistics for NADK2 SeMet

Human NAD kinase 2 (47-442) SeMet • NAD^+	
Data collection	
Space Group	$C222_1$
Cell dimensions	
a, b, c (Å)	97.13, 118.12, 188.63
α, β, γ (^{O})	90.0, 90.0, 90.0
Resolution (Å)	30-2.80 (2.91-2.80)
R_{pim}	0.035 (0.198)
CC(1/2)	0.997 (0.932)*
$I/\sigma I$	13.9 (3.3)*
Completeness (%)	99.9 (100.0)
Redundancy	14.0 (14.7)
Refinement	
Resolution (Å)	30 - 2.80 (2.87 - 2.80)*
No. unique reflections	42223
R_{work}/R_{free}	0.191 (0.194)/ 0.249 (0.263)
No. atoms	10869
Protein	10490
NAD	176
Water	203
B-factors	
Protein	55.8
NAD/Water	48.49
R.m.s deviations	
Bond lengths (Å)	0.008
Bond angles (^{O})	1.026
Ramachandran plot (%)	
Favored	95.5
Outliers	0.2

Highest-resolution shell is shown in parentheses.
*High resolution limit of 2.8 Å was chosen conservatively due to weaker than average density for chain D.

References

1. Y. Fukasawa *et al.*, MitoFates: improved prediction of mitochondrial targeting sequences and their cleavage sites. *Mol Cell Proteomics* **14**, 1113-1126 (2015).
2. G. Hoxhaj *et al.*, Direct stimulation of NADP(+) synthesis through Akt-mediated phosphorylation of NAD kinase. *Science* **363**, 1088-1092 (2019).
3. M. A. Estrella *et al.*, The metabolites NADP(+) and NADPH are the targets of the circadian protein Nocturnin (Curled). *Nat Commun* **10**, 2367 (2019).
4. W. Kabsch, XDS. *Acta Crystallogr D Biol Crystallogr* **66**, 125-132 (2010).
5. P. Evans, Scaling and assessment of data quality. *Acta Crystallogr D Biol Crystallogr* **62**, 72-82 (2006).
6. G. M. Sheldrick, Experimental phasing with SHELXC/D/E: combining chain tracing with density modification. *Acta Crystallogr D Biol Crystallogr* **66**, 479-485 (2010).
7. C. B. Hübschle, G. M. Sheldrick, B. Dittrich, ShelXle: a Qt graphical user interface for SHELXL. *J Appl Crystallogr* **44**, 1281-1284 (2011).
8. P. Emsley, K. Cowtan, Coot: model-building tools for molecular graphics. *Acta Crystallogr D Biol Crystallogr* **60**, 2126-2132 (2004).
9. P. D. Adams *et al.*, PHENIX: building new software for automated crystallographic structure determination. *Acta Crystallogr D Biol Crystallogr* **58**, 1948-1954 (2002).
10. E. F. Pettersen *et al.*, UCSF Chimera--a visualization system for exploratory research and analysis. *J Comput Chem* **25**, 1605-1612 (2004).
11. E. Gasteiger *et al.*, ExPASy: The proteomics server for in-depth protein knowledge and analysis. *Nucleic Acids Res* **31**, 3784-3788 (2003).

A

Presequence

- Possessing mitochondrial presequence (Precision:0.83, Recall:0.73)
- Possessing mitochondrial presequence (Precision:0.79, Recall:0.80)
- No mitochondrial presequence

Cleavage site

- MPP cleavage site
- Oct1 cleavage site
- Icp55 cleavage site

Motif

- TOM20 recognition motif (ΦχβΦΦ)
- Max positively charged amphiphilicity (PA) score region (high)
- Max positively charged amphiphilicity (PA) score region (low)

Φ β σ γ Reduced letters composing statistically significant 6mer in presequence
Φ(hydrophobic), β(basic), σ(polar), γ(secondary structure breaker)

Results in text

Sequence ID	Probability of presequence	Cleavage site (processing enzyme)	Net charge	Sequence (100 amino acids from N terminal)
sp|Q4G0N4|NAKD2_HUMAN NAD kinase 2, mitochondrial OS=Homo sapiens OX=9606 GN=NADK2 PE=1 SV=2	0.604	46 MPP	0.152	MTCYRGFLLGSCCRVAGGRAAALRGPGAGGPAARPRLGGDGGGRRHLGQGQPRELAGCG

B

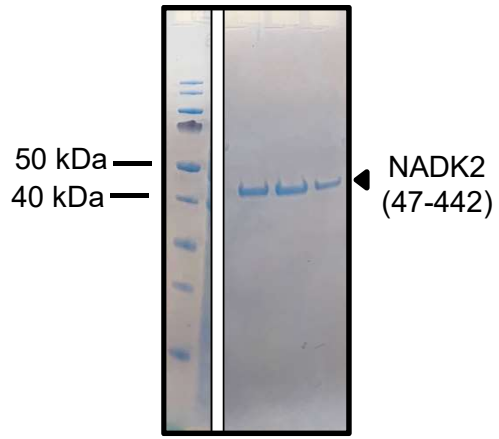

Fig. S1

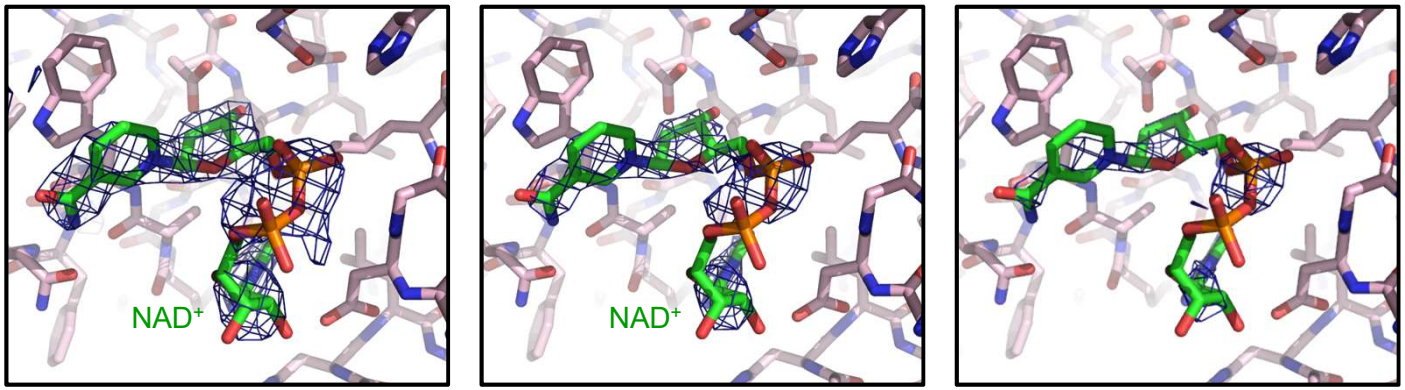

SA 2000K Fo-Fc 4σ | 5σ | 6σ

Fig. S2

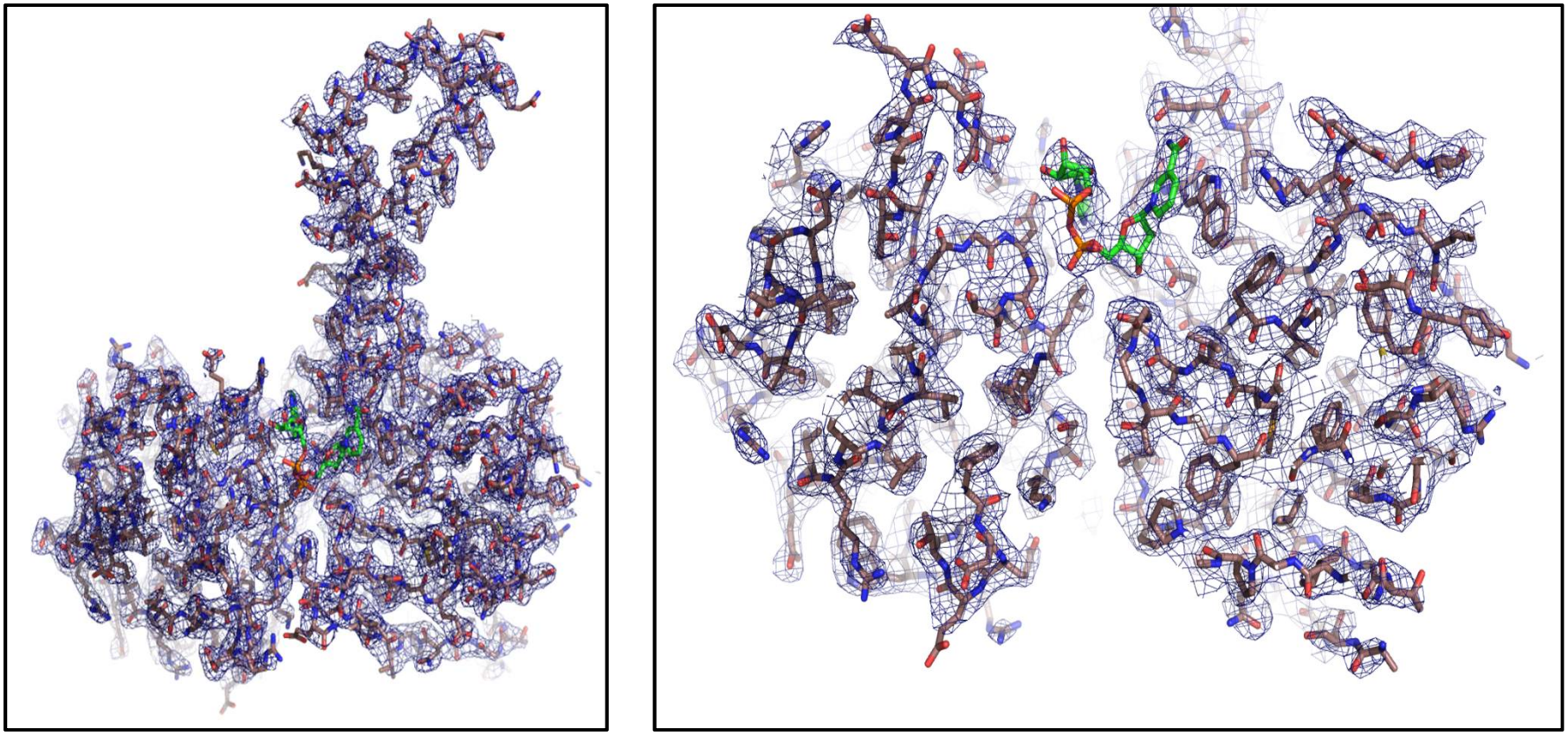

2Fo-Fc 1σ

Fig. S3

A

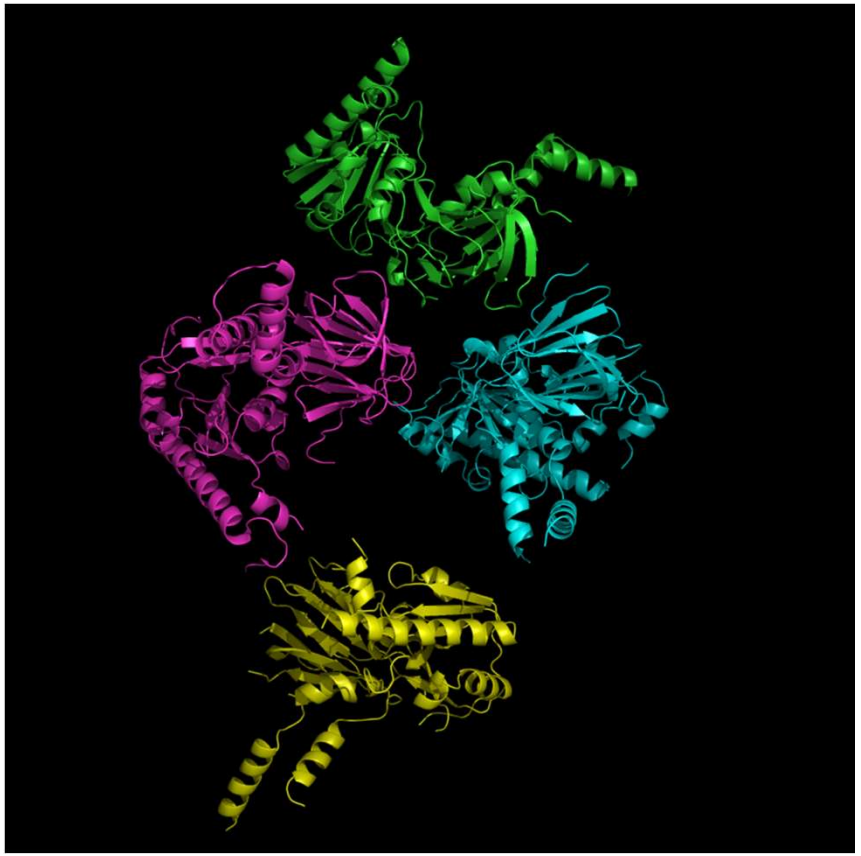

Asymmetric unit (ASU)

B

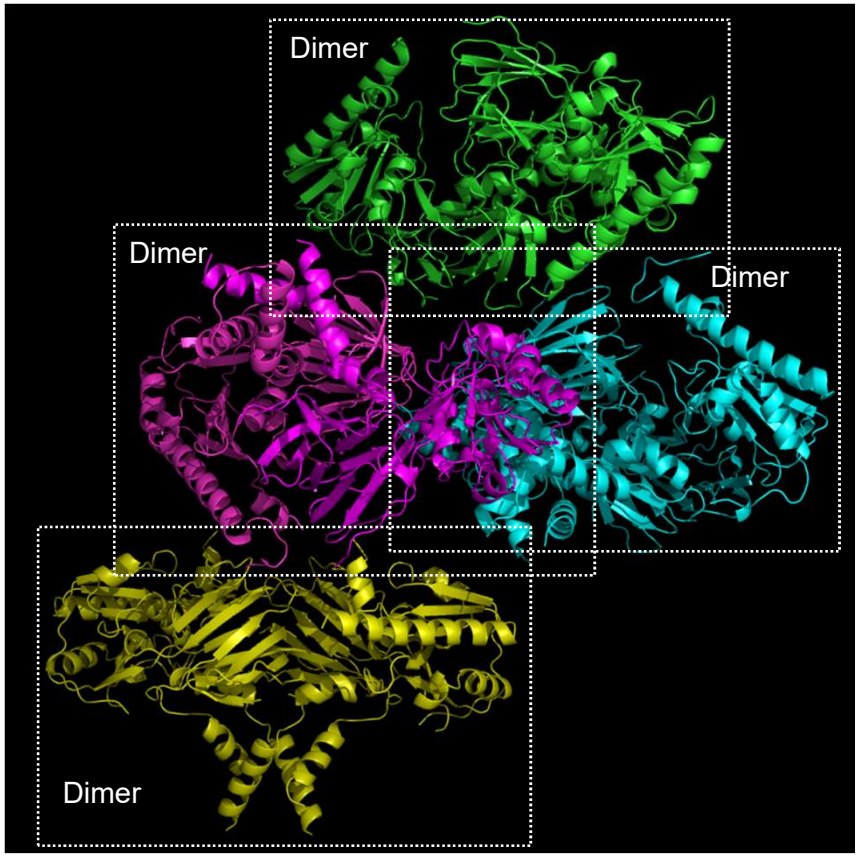

ASU + symmetry mates

Fig. S4

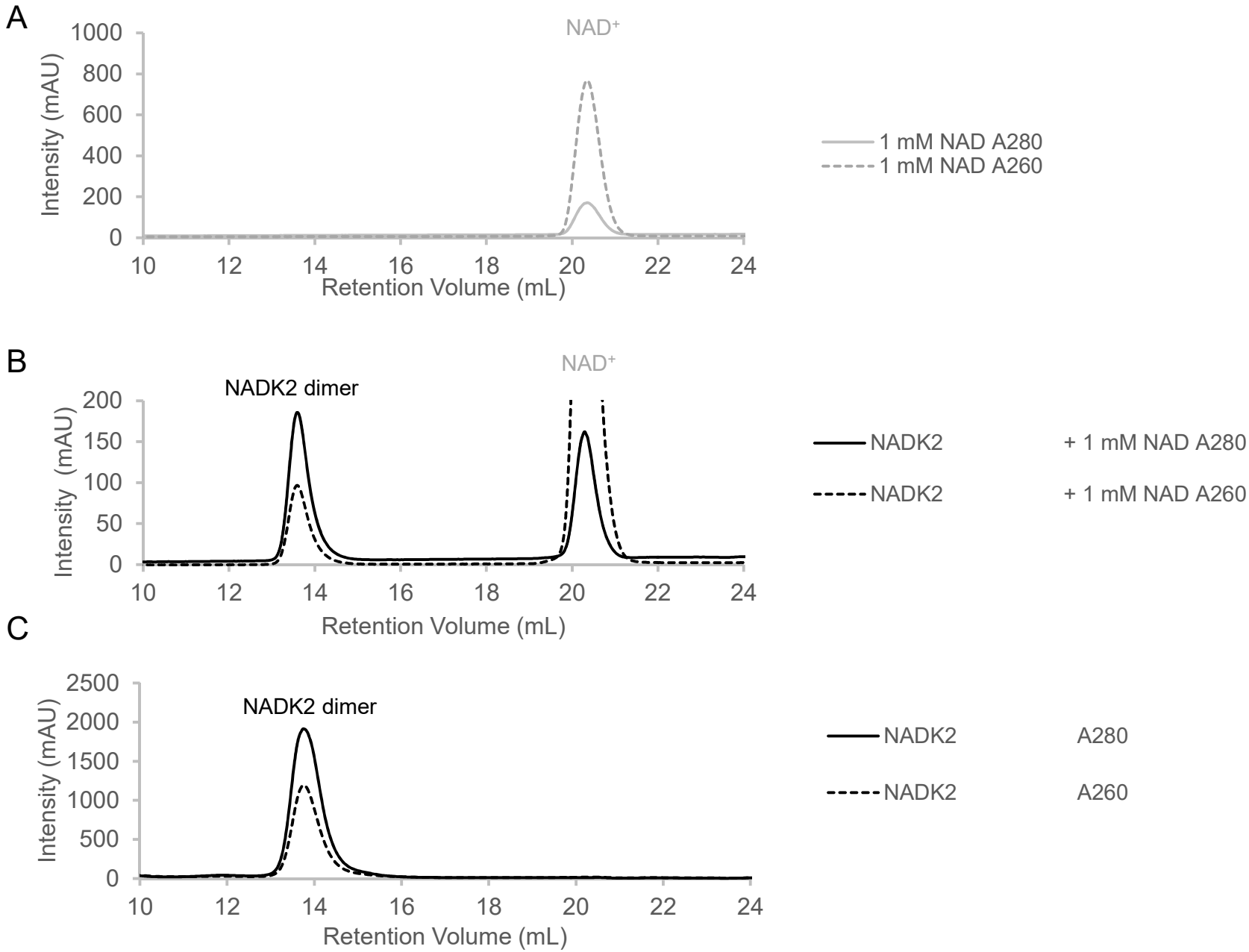
A
NAD+
Intensity (mAU)
1000
800
600
400
200
0
10
12
14
16
18
20
22
24
Retention Volume (mL)
1 mM NAD A280
1 mM NAD A260
B
NAD+
NADK2 dimer
Intensity (mAU)
200
150
100
50
0
Retention Volume (mL)
NADK2 + 1 mM NAD A280
NADK2 + 1 mM NAD A260
C
NADK2 dimer
Intensity (mAU)
2500
2000
1500
1000
500
0
Retention Volume (mL)
NADK2 A280
NADK2 A260

Fig. S5

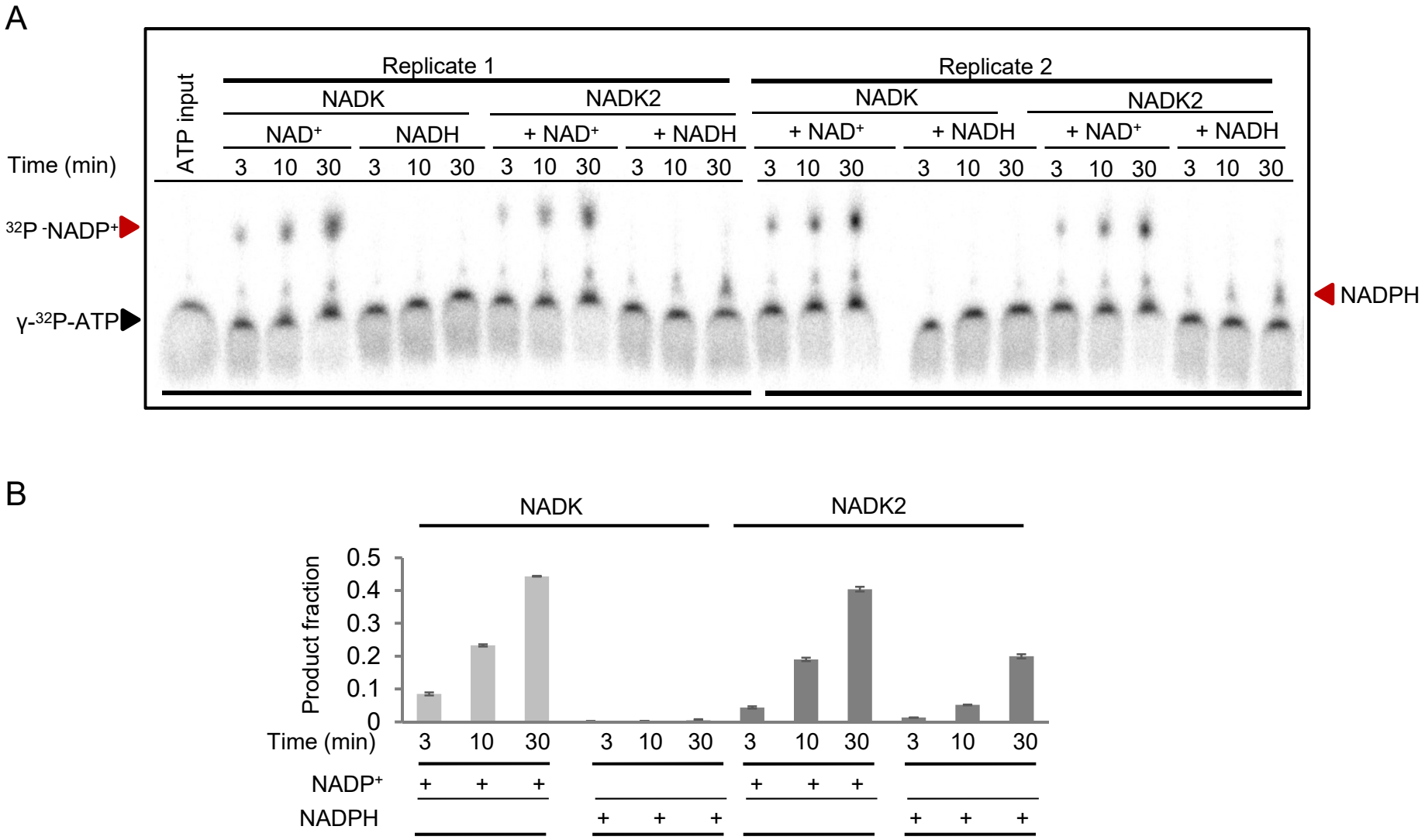
A
Replicate 1
Replicate 2
NADK
NADK2
NADK
NADK2
ATP input
NAD+
NADH
+ NAD+
+ NADH
+ NAD+
+ NADH
+ NAD+
+ NADH
Time (min)
3 10 30 3 10 30 3 10 30 3 10 30 3 10 30 3 10 30 3 10 30 3 10 30
32P -NADP+
γ-32P-ATP
NADPH
B
NADK
NADK2
Product fraction
0.5
0.4
0.3
0.2
0.1
0
Time (min)
3 10 30 3 10 30 3 10 30 3 10 30
NADP+
+ + + + + +
NADPH
+ + + + + +

Fig. S6

A

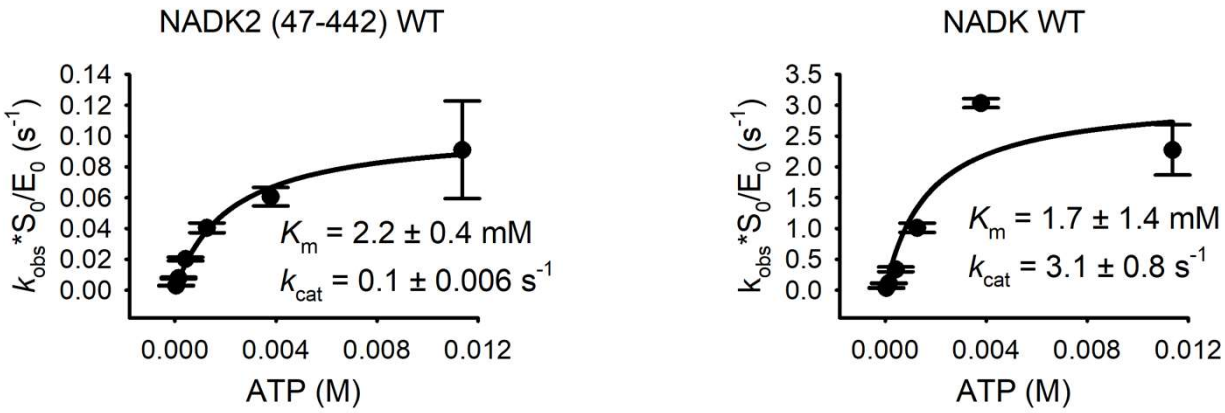
NADK2 (47-442) WT
k_{obs}*S_0/E_0 (s^{-1})
0.14
0.12
0.10
0.08
0.06
0.04
0.02
0.00
K_m = 2.2 ± 0.4 mM
k_{cat} = 0.1 ± 0.006 s^{-1}
0.000
0.004
0.008
0.012
ATP (M)
NADK WT
k_{obs}*S_0/E_0 (s^{-1})
3.5
3.0
2.5
2.0
1.5
1.0
0.5
0.0
K_m = 1.7 ± 1.4 mM
k_{cat} = 3.1 ± 0.8 s^{-1}
0.000
0.004
0.008
0.012
ATP (M)

B

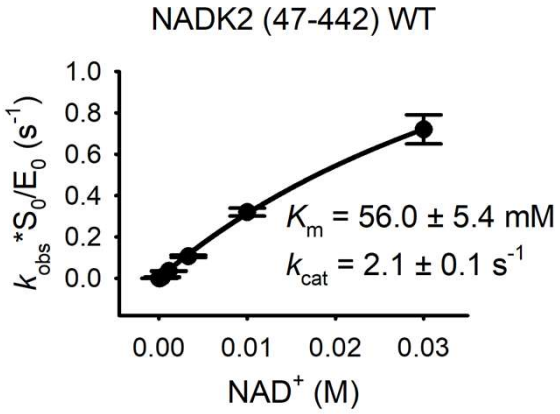
NADK2 (47-442) WT
k_{obs}*S_0/E_0 (s^{-1})
1.0
0.8
0.6
0.4
0.2
0.0
K_m = 56.0 ± 5.4 mM
k_{cat} = 2.1 ± 0.1 s^{-1}
0.00
0.01
0.02
0.03
NAD^+ (M)

Fig. S7

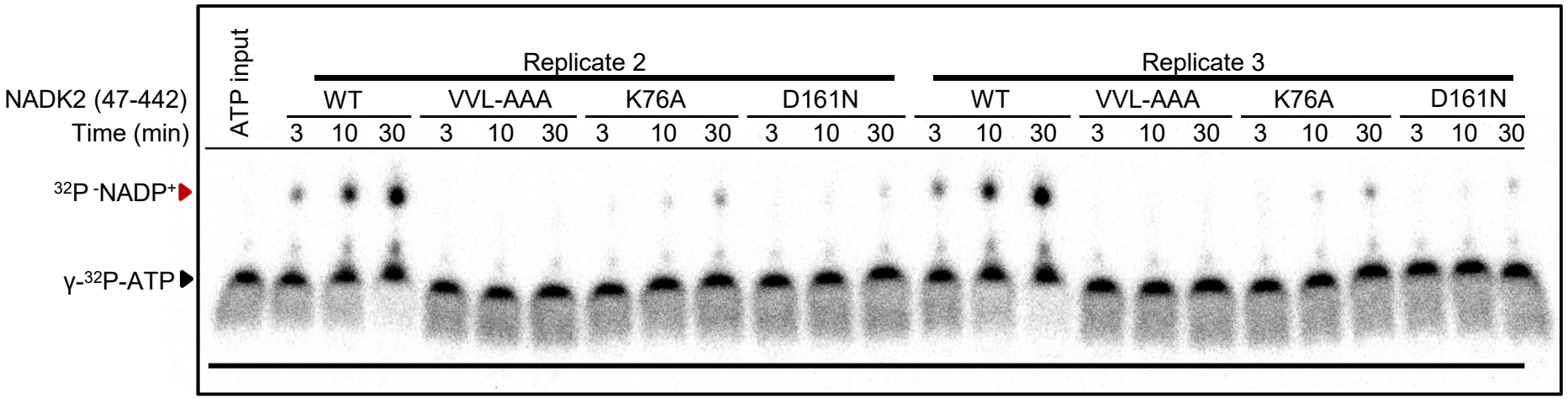
ATP input
Replicate 2
Replicate 3
NADK2 (47-442)
WT
VVL-AAA
K76A
D161N
Time (min)
3 10 30
^{32}P -NADP^{+}
γ-^{32}P-ATP

Fig. S8

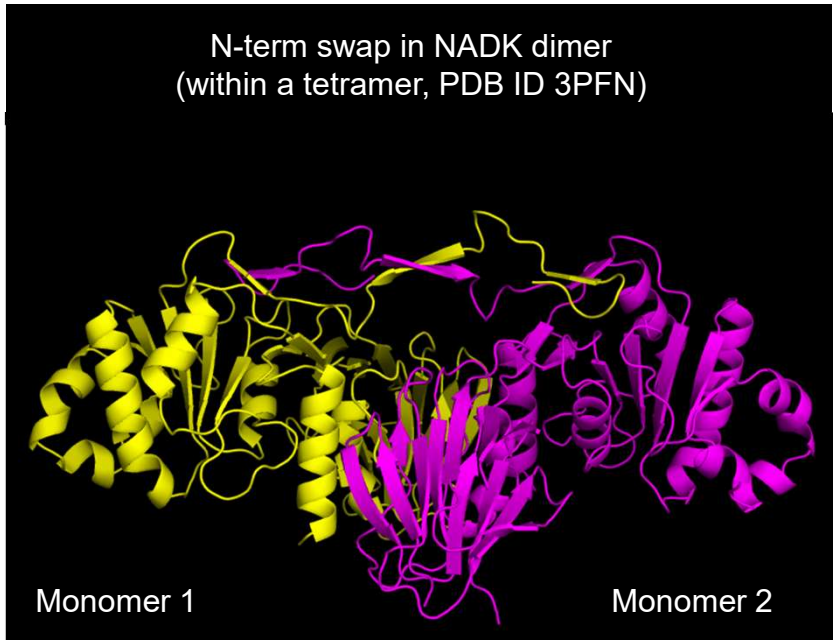
N-term swap in NADK dimer
(within a tetramer, PDB ID 3PFN)
Monomer 1
Monomer 2

Fig. S9